Histol Histopathol (2018) 33: 1111-1123

http://www.hh.um.es

Histology and Histopathology

From Cell Biology to Tissue Engineering

Butylated hydroxytoluene induces type-V collagen and overexpression of remodeling genes/proteins in experimental lung fibrosis

Vanessa Martins[1], Walcy Rosolia Teodoro[2], Ana Paula Pereira Velosa[2], Priscila Andrade[2], Cecília Farhat[1], Alexandre Todorovic Fabro[3] and Vera Luiza Capelozzi[1]

[1]Department of Pathology, [2]Rheumatology Discipline, Faculty of Medicine and [3]Ribeirão Preto Medical School, University of São Paulo, São Paulo, Brazil

Summary. Anomalous histoarchitecture with increased levels of type-V collagen (Col V) in lungs of human idiopathic pulmonary fibrosis (IPF) and bleomycin (BLM) airway-centered interstitial fibrosis suggest that this collagen can be a possible trigger involved in the pathogenesis of these diseases. Butylated hydroxytoluene (BHT) injury model revealed a distal involvement of lung parenchyma with significant endothelial injury and fibrotic response, contrasting with the BLM airway-centered insult. We undertook this study to analyze whether BHT alters distal airway/alveolar epithelial cells (AECs) and extracellular matrix (ECM) signaling involved in the initiation and progression of pulmonary fibrosis in a different pathway concerning overexpression of Col V. Female mice C57BL/6 (n=6) were instilled intraperitoneally with 400mg/kg of BHT dissolved in 1 mL of corn oil and euthanized at day 14 or 21 after BHT administration. Morphometry, immunohistochemistry and transmission electron microscopy were performed to characterize microscopic and submicroscopic changes of AECs and endothelial cells through transforming growth factor beta (TGF-β) basic fibroblast growth factor (bFGF) and vascular endothelial growth factor (VEGF) expression. Immunofluorescence and immunogold electron microscopy were performed to characterize Col V. Quantitative polymerase chain reaction (qPCR) was used to confirm differential levels of RNA messenger. BHT lungs showed marked fibrotic areas and hyperplastic AECs. The alveolar damage caused destruction of elastic fibers and a critical increase of Col V in ECM of distal lung parenchyma. Fibrogenesis-promoting markers TGF-β, bFGF and VEGF were also overexpressed *in situ*, coinciding with up-regulation in remodeling enzymes, growth factors, cytokines, transduction and transcription genes. BHT alters distal lung parenchyma signaling involved in pulmonary fibrosis highlighted similarities to human IPF in a pathway involving Col V arising as a promissory model to identify effective therapeutic targets.

Key words: Pulmonary fibrosis, Butylated hydroxytoluene, Extracellular matrix, Type-V collagen, RT-PCR, Immunohistochemistry, Immunofluorescence, Electron microscopy

Offprint requests to: Prof. Vera Luiza Capelozzi, Department of Pathology, Faculdade de Medicina da Universidade de São Paulo, Av. Dr. Arnaldo 455, room 1143, ZIP CODE 01296-903, São Paulo, SP, Brazil. e-mail: vera.capelozzi@fm.usp.br

DOI: 10.14670/HH-18-010

Introduction

Lung fibrosis is a final response to a variety of lung injuries characterized by epithelial/endothelial cell damage, increase of the fibroblast/myofibroblast population and abnormal accumulation of extracellular matrix (ECM) replacing normal parenchyma (Pardo and Selman, 2002). The specific functional and biochemical properties of the lung replaced by fibrosis are based on the deposition of collagen (Col) V, Col I and Col III, which co-assemble into a unique macromolecule to form heterotypic fibers (Birk et al., 1990; Gelse et al., 2003). Type-V collagen is the minor component of these fibers

and is found between Col I and Col III fibers. Only its amino-terminal portion, which regulates the diameter of heterotypic fibers, projects to the outer surface, contributing to the development of functional properties of connective tissues (Roulet et al., 2007). Type-V collagen is present in the basement membrane (BM) of airways and alveolar walls synthetized by smooth muscle and endothelial cells (Konomi et al., 1984). We previously observed an increased Col V expression in lungs of idiopathic pulmonary fibrosis (IPF) and systemic sclerosis and patients and, of note, high deposition of this protein was associated with reduced vital capacity and diffusing capacity for carbon-monoxide, indicating that this protein has a role in lung tissue fibrotic disorders (Parra et al., 2009, 2010). More recently, Fabro and colleagues (Fabro et al., 2015) reported an increased expression of thickened Col V in lungs of BLM fibrosis, similar to human airway-centered interstitial fibrosis (Churg et al., 2004).

Although various causes of lung fibrosis result in a uniform pathology, evidence indicates that the pathophysiology may differ according to the type of the primary insult (Churg et al., 2004; Song et al., 2009). Two different forms of primary insult are described: airway-centered, with direct effects on lung epithelial cells, and peripheral, reflecting lung involvement secondary to a systemic inflammatory response, being the main target damage to the pulmonary endothelial cell (Churg et al., 2004; Song et al., 2009). It has been recognized that proximal airway-centered and distal lung fibrosis are not identical, and differences could be detected radiographically, functionally, and therapeutically (Song et al., 2009). To rule out these differences and to better understand the mechanisms regulating the fibroproliferative responses, we previously evaluated an injury model with butylated hydroxytoluene (BHT). The histology from this injury model revealed a distal involvement of lung parenchyma (Parra et al., 2008) with significant endothelial injury and fibrotic response, contrasting with the airway-centered insult to pulmonary epithelium yielded more pronounced inflammatory responses in BLM animals (Fabro et al., 2015). Because which both studies analyzed only morphological changes after the induction of lung injury, we could not assert whether altered distal airway/alveolar epithelial cell and mesenchyme signaling molecular mechanisms are likely to be differently implicated in airway-centered and peripheral fibrosis

In light of these previous reports, we hypothesize that BHT alters distal airway/alveolar epithelial cells and extracellular matrix signaling involved in the initiation and progression of pulmonary fibrosis in a different pathway involving overexpression of Col V and remodeling regulated genes/proteins. Thus, we extended our investigation with the aim to (1) document the time-related perpetuation of BHT-induced lung fibrosis and 2) to determine Col V gene expression and response protein patterns associated with the initial progression and the subsequent stabilization of the fibrotic response.

Material and methods

Animals and experimental protocol

Female C57BL/6 mice (n=6) 6-7 weeks old were instilled intraperitoneally (i.p.) with 400mg/kg of BHT (Sigma Chemical Company, USA) dissolved in 1 mL of corn oil (Haschek et al., 1983; Parra et al., 2008). Control group received the same volume of corn oil. The mice were placed in a ventilated Plexiglas chamber with a mixture of pure humidified oxygen and compressed air to maintain the oxygen concentration at 70%. An oxygen analyzer periodically monitored this concentration. Six days later, the animals were transferred to room air where they were kept for the remainder of the experiment. All animals are provided from animal facility of our institution and maintained in specific pathogen-free conditions with free access to food and fresh water in a temperature controlled room (22-24°C) in a 12h light/dark cycle. All experimental procedures were performed according to The Committee on Ethical Use of Laboratory Animals of Faculty of Medicine of University of São Paulo (process code: 372/11). For analysis, mice were euthanized at day 14 or 21 after BHT administration.

Specimen preparation

After BHT administration, mice were euthanized and after a midline thoracotomy, the trachea was cannulated, and the lungs were fixed by instillation of 0.5 mL of buffered formalin (10%), at a pressure of 18-22 cm H_2O, for one to two minutes. The trachea was then ligated, and the lungs, separated from the heart, were immersed in buffered formalin (10%) solution for 48 hours. The left lung was embedded in paraffin, sliced (5μm) perpendicularly to the lung base (apico-basal axis), giving origin to 2 halves with portions of the upper, middle, and base of the lung, and stained with hematoxylin-eosin (H&E), Masson's Trichome and Resorcin-fuchsin staining.

Hydroxyproline assay

Lung collagen deposition was estimated by measuring the hydroxyproline content as previously described with modifications (Vittal et al., 2013). Briefly, the lungs portions were freeze-dryed (Edwards, Modulyo), weighed and hydrolyzed in 6 N HCl for 22 hours at 110°C. Lung hydroxyproline levels were determined spectrophotometrically by absorbance at 560nm and the results were expressed as ng hydroxyproline per mg of protein (Vittal et al., 2013).

Transmission electron microscopy

Transmission electron microscopy was performed in all groups. Small blocks (1 mm^3) of lungs were fixed in a solution of 2% glutaraldehyde in sodium phosphate

and potassium 0.15 M buffer, pH 7. Material was fixed en bloc in aqueous uranyl acetate for 24 hours. After this procedure, the samples were dehydrated in acetone, and were embedded in Araldite resin. Ultrathin sections were obtained with a diamond knife on LKB Ultratome microtome (Leica, Deerfield, IL, USA). Subsequently, they were placed on copper grid (200-mesh; Lab Research Industries, Burlington, VT, USA), and counterstained with uranyl acetate and lead citrate. Micrographs were taken at 80 kV with Transmission Electron Microscope JEOL 100cx 100KW (Philips, Munich, Germany).

Immunogold electron microscopy

BHT and control lung samples were fixed in 2% glutaraldehyde for 2 hours at room temperature. Subsequently, the specimens were dehydrated in increasing concentrations of ethanol, and embedded in the LR White acrylic resin (London Resin Company, London, UK) for 1 hour. After this period, the samples were immersed in gelatin capsules for subsequent polymerization and attainment of the semi-thin (2 μm) cuts. After staining with toluidine blue to verify the preservation of the histological pattern, the specimens were sectioned in 50nm thick-ultrathin sections and were placed on nickel screen. For ultrastructural immunolocalization by simple indirect labeling, specimen sections were hydrated in water, and to block nonspecific sites incubated with Tris buffered saline (TBS) containing 0.02 M glycine, pH 7.4, and normal goat serum. Then, the sections were incubated for 12 hours at 4°C with polyclonal mouse antihuman-Col V (1:30) diluted in TBS containing 0.1% BSA and 0.05% $Tween_{20}$, pH 7.4. After this, washing was performed with TBS/BSA for 5 minutes. Subsequently, the 5nm colloidal gold-conjugated anti-mouse IgG and 5nm colloidal gold-conjugated anti-rabbitt IgG (Sigma Chemical Co., St. Louis, MO, USA) were diluted 1:50 in 0.5M NaCl/0.1% BSA with 0.05% $Tween_{20}$, pH 8.0 and incubated for two hours at room temperature. After washing cycles with TBS/0.1% BSA with 0.05% $Tween_{20}$, pH 8.0, fixation of the sections was performed in 2.5% glutaraldehyde diluted in 0.1 M sodium cacodylate buffer, pH 7.4. Finally, the sections were washed in distilled water, counterstained with uranyl acetate and lead nitrate and examined in a transmission electron microscope JEOL 100CX 100KW (Philips, Munich, Germany).

Immunohistochemistry

To evaluate epithelial involvement, expression of epithelial regulatory proteins and endothelium activation we used immunohistochemistry. Sections were deparaffinized, hydrated and the slides were incubated with 10 mM sodium citrate. Endogenous peroxidase activity was blocked with 3% hydrogen peroxide. Slides were washed in TBS with 0.05% Tween-20 (Sigma, St. Louis, MO) and blocked with serum-free protein block (Dako, Carpinteria, CA). Antibody for basic fibroblast growth factor (bFGF) (Upstate; 1:150 dilution); transforming growth factor (TGF-β) (Santa Cruz; 1:3000 dilution) and vascular endothelial growth factor (VEGF) (Santa Cruz; 1:1000 dilution) were diluted in TBS/Tween buffer and incubated overnight at 4°C. Reactions were immunostained with Vectastain ABC (Vector Laboratories, Inc., Burlingame, CA). Color was developed with 3,3-diaminobenzidinetetra-hydrochloride (Vector Laboratories, Inc.), and counterstained with H&E. An isotype immunoglobulin G (IgG) was used as negative control.

Histomorphometry

To access uniform and proportional lung samples, 10 fields (five non-overlapping fields in two different sections) were randomly analyzed in proximal and distal lung parenchyma (airways and AECs). The measurements were done with a 100-point and 50 straight grid with a known area (62.500 mm^2 at a 400x magnification) attached to the ocular of the microscope (Gundersen et al., 1988; Weibel, 2017). At 400x magnification, the area in each field was calculated according to the number of points hitting positive cells for specific antibody as a proportion of the total grid area. Bronchi and blood vessels were carefully avoided during the measurements. In order to normalize the data, the area occupied by specific antibody, measured in each field, was divided by the length of each septum studied (to avoid any bias secondary to septal edema, alveolar collapse and denser tissue matrix seen in the fibrotic sections). The results express the fractional area of positive cells determined as the number of positive cells in each field divided by the connective tissue area. The results were expressed in percent (Gundersen et al., 1988; Weibel, 2017).

Immunofluorescence

To identify Col I, Col III and Col V we employed immunofluorescence. The sections of all groups were washed in xylene and were dehydrated in graded ethanol. Antigen retrieval was done by enzymatic treatment of lungs with bovine pepsin (10000 UTD) (Sigma Chemical Co.) in 0.5N acetic acid buffer (pH=2.5) (4 mg/mL) for 30 minutes at 37°C and subsequent incubation with 5% bovine serum albumin (BSA) in PBS was performed. The slides were then incubated overnight at 4°C with rabbit polyclonal antibody anti-collagen type I (1:100, Rockland, Limerick, PA, USA), anti-collagen type III (1:100, Rockland, Limerick, PA, USA) and anti-collagen type V (1:2000). For negative controls, sections were incubated with fetal bovine serum instead of the primary antibody. Finally, the sections were incubated with a goat anti-rabbit immunoglobulin ALEXA 488 (dilution 1:200; Invitrogen, Life Technologies, Thermo Fisher Scientific, Rockford, IL), diluted in PBS containing 0.0006% Evans Blue and mounted with 3-aminopropyltriethoxysilane

(Sigma Chemical Co., St. Louis, MO, USA). Collagenous fibers were quantified by optical density at the image analysis system (Image Pro-Plus 6.0) in ten different, randomly selected alveolar septa, as previously described by our group (Parra et al., 2008). The results were expressed as the percentage of the alveolar septal area fraction occupied by the fibers of the collagenous.

Quantitative RT- PCR array

Total RNA was isolated from lung using RNase Microarray Tissue, from Qiagen (cat. No. 73304). First-strand cDNA was synthesized using a RT2 First Strand kit from Qiagen (cat. No. 330401). The mouse fibrosis PCR Array-RT2 Profiler Arrays (SABiosciences; Qiagen, Valencia, CA), containing 84 genes (Table 1) was used according to the manufacturer's instructions. Array data were analyzed using 2-[Delta Delta C(T)] $2(^{-\Delta\Delta CT})$ methodology.

Statistical analysis

Statistical differences between groups were determined by one-way ANOVA followed by post hoc

Table 1. Genes present on the plate of the RT2-PCR assay array from Qiagen.

Symbol	Description
Acta2	Actin, alpha 2, smooth muscle, aorta
Agt	Angiotensinogen (serpin peptidase inhibitor, clade A, member 8)
Akt1	Thymoma viral proto-oncogene 1
Bcl2	B-cell leukemia/lymphoma 2
Bmp7	Bone morphogenetic protein 7
Cav1	Caveolin 1, caveolae protein
Ccl11	Chemokine (C-C motif) ligand 11
Ccl12	Chemokine (C-C motif) ligand 12
Ccl3	Chemokine (C-C motif) ligand 3
Ccr2	Chemokine (C-C motif) receptor 2
Cebpb	CCAAT/enhancer binding protein (C/EBP), beta
Col1a2	Collagen, type I, alpha 2
Col3a1	Collagen, type III, alpha 1
Ctgf	Connective tissue growth factor
Cxcr4	Chemokine (C-X-C motif) receptor 4
Dcn	Decorin
Edn1	Endothelin 1
Egf	Epidermal growth factor
Eng	Endoglin
Fasl	Fas ligand (TNF superfamily, member 6)
Grem1	Gremlin 1
Hgf	Hepatocyte growth factor
Ifng	Interferon gamma
Il10	Interleukin 10
Il13	Interleukin 13
Il13ra2	Interleukin 13 receptor, alpha 2
Il1a	Interleukin 1 alpha
Il1b	Interleukin 1 beta
Il4	Interleukin 4
Il5	Interleukin 5
Ilk	Integrin linked kinase
Inhbe	Inhibin beta E
Itga1	Integrin alpha 1
Itga2	Integrin alpha 2
Itga3	Integrin alpha 3
Itgav	Integrin alpha V
Itgb1	Integrin beta 1 (fibronectin receptor beta)
Itgb3	Integrin beta 3
Itgb5	Integrin beta 5
Itgb6	Integrin beta 6
Itgb8	Integrin beta 8
Jun	Jun oncogene
Lox	Lysyl oxidase
Ltbp1	Latent transforming growth factor beta binding protein 1
Mmp13	Matrix metallopeptidase 13
Mmp14	Matrix metallopeptidase 14 (membrane-inserted)
Mmp1a	Matrix metallopeptidase 1a (interstitial collagenase)
Mmp2	Matrix metallopeptidase 2
Mmp3	Matrix metallopeptidase 3
Mmp8	Matrix metallopeptidase 8
Mmp9	Matrix metallopeptidase 9
Myc	Myelocytomatosis oncogene
Nfkb1	Nuclear factor of kappa light polypeptide gene enhancer in B-cells 1, p105
Pdgfa	Platelet derived growth factor, alpha
Pdgfb	Platelet derived growth factor, B polypeptide
Plat	Plasminogen activator, tissue
Plau	Plasminogen activator, urokinase
Plg	Plasminogen
Serpina1a	Serine (or cysteine) peptidase inhibitor, clade A, member 1a
Serpine1	Serine (or cysteine) peptidase inhibitor, clade E, member 1
Serpinh1	Serine (or cysteine) peptidase inhibitor, clade H, member 1
Smad2	MAD homolog 2 (Drosophila)
Smad3	MAD homolog 3 (Drosophila)
Smad4	MAD homolog 4 (Drosophila)
Smad6	MAD homolog 6 (Drosophila)
Smad7	MAD homolog 7 (Drosophila)
Snai1	Snail homolog 1 (Drosophila)
Sp1	Trans-acting transcription factor 1
Stat1	Signal transducer and activator of transcription 1
Stat6	Signal transducer and activator of transcription 6
Tgfb1	Transforming growth factor, beta 1
Tgfb2	Transforming growth factor, beta 2
Tgfb3	Transforming growth factor, beta 3
Tgfbr1	Transforming growth factor, beta receptor I
Tgfbr2	Transforming growth factor, beta receptor II
Tgif1	TGFB-induced factor homeobox 1
Thbs1	Thrombospondin 1
Thbs2	Thrombospondin 2
Timp1	Tissue inhibitor of metalloproteinase 1
Timp2	Tissue inhibitor of metalloproteinase 2
Timp3	Tissue inhibitor of metalloproteinase 3
Timp4	Tissue inhibitor of metalloproteinase 4
Tnf	Tumor necrosis factor
Vegfa	Vascular endothelial growth factor A
Actb	Actin, beta
B2m	Beta-2 microglobulin
Gapdh	Glyceraldehyde-3-phosphate dehydrogenase
Gusb	Glucuronidase, beta
Hsp90ab1	Heat shock protein 90 alpha (cytosolic), class B member 1
MGDC	Mouse Genomic DNA contamination
RTC	Reverse Transcription Control
RTC	Reverse Transcription Control
RTC	Reverse Transcription Control
PPC	Positive PCR Control
PPC	Positive PCR Control
PPC	Positive PCR Control

Table 1. Continuation.

analysis using Bonferroni test for area fraction of inflammation, fibrosis, immunohistochemistry and immunofluorescence markers, as well as quantitative PCR and hydroxyproline measurement. Results are expressed as mean ± SEM. Hierarchical clustering on this set was done as follows: gene values were normalized by subtracting the means of the signal intensities for each gene; the distance metric used was d=(1-p)/2, where p is the Pearson correlation function between samples. The Ward linkage method was used. Statistical significance was set at P less than 0.05.

Results

BHT induces peripheral alveolar collapse, inflammation and fibrosis

Figure 1 shows lung tissue sections of saline- and BHT-instilled mice stained with hematoxylin-eosin, Masson trichrome, resorcin-fuchsin, and immunohistochemistry, respectively. Histopathologic examination shows that control mice presented a normal lung architecture (Fig. 1A,E,I) whereas BHT (Fig. 1B,F,C,G) promotes substitution of the distal alveoli by extensive parenchyma scarring. 14 days after BHT treatment, lungs show severe edema and large numbers of inflammatory cells (Fig. 1B) followed at 21 days by marked fibrotic areas, alveolar collapse and hyperplastic epithelial cells (Fig. 1C). The permanent alveolar damage causes significant destruction of alveolar elastic fibers (Fig. 1J,K,L; P<0.05) and a critical increase of ECM deposition in distal lung parenchyma (Fig. 1D,H; P<0.05).

Figure 2 shows the analysis of lung tissue sections of saline- and BHT-instilled mice stained with immunoperoxidase. Compared to control critical fibrogenesis-promoting growth factors such as TGF-β (Fig. 2A), bFGF (Fig. 2B) and VEGF (Fig. 2C) were

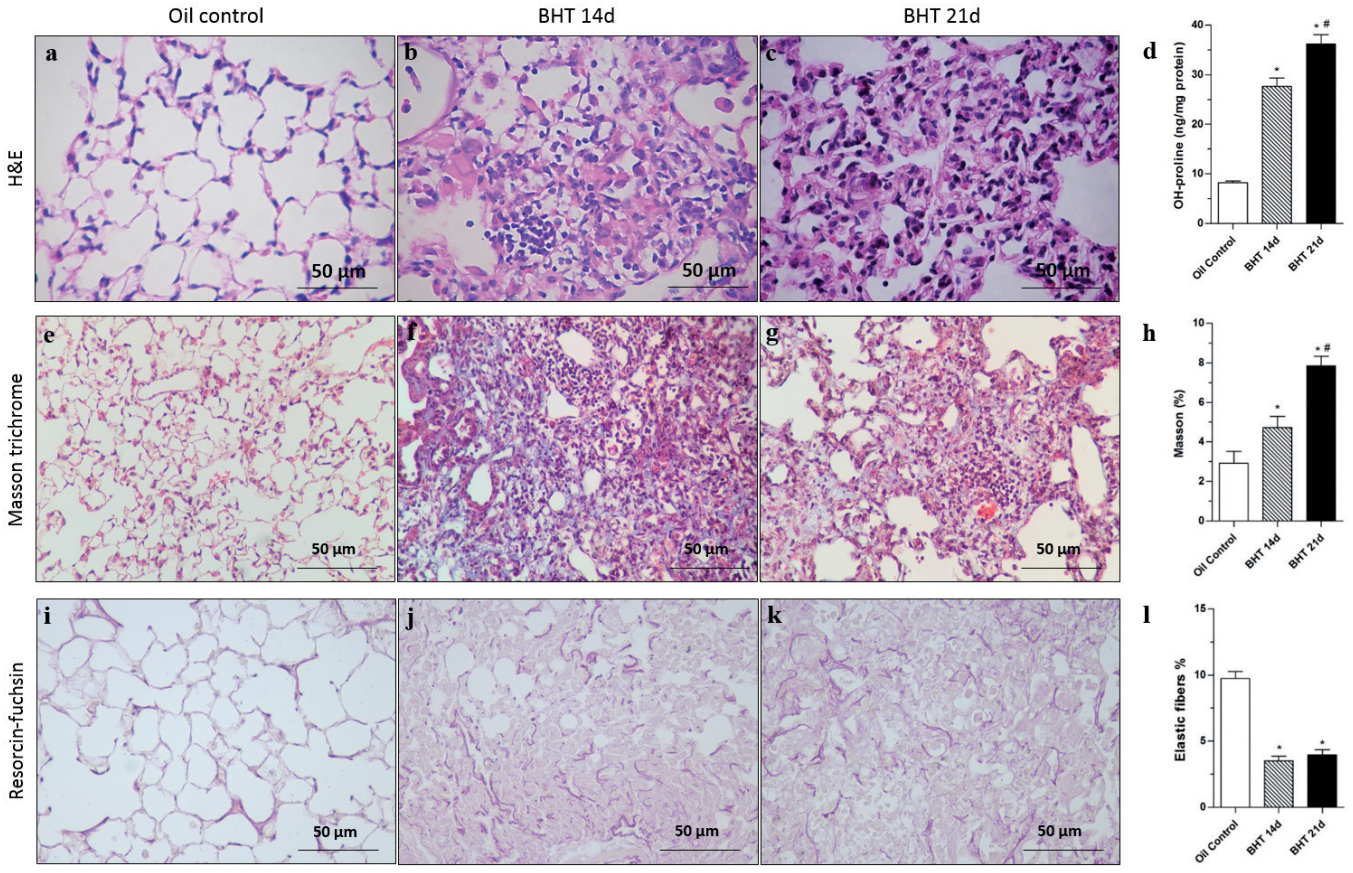

Fig. 1. Histological assessment, collagen content, elastic fibers and immunohistochemistry in lung tissue during the time course of BHT-induced lung fibrosis. **A-C, E-G, I-K.** Representative light micrographs in lung tissue sections of saline- and BHT-instilled mice stained with hematoxylin-eosin, Masson Trichrome and Resorcin-Fuchsin, respectively. **A, E, I.** Saline-instilled mouse. **B-C, F-G, J-K.** BHT-instilled mice at 14, and 21 days, respectively. Histopathology shows inflammation and areas of lung fibrosis at 14 days coincident with disarrangement of elastic fibers with a more severe and diffused fibrotic reaction at 21 days allied to the distortion of pulmonary histoarchitecture and large, sparse and fragmented bundles of elastic system. **D, H, L.** Fibrosis, elastosis and collagen quantitation. *Compared to oil control, #compared to BHT14d; P<0.05. Scale bars: 50 μm.

significantly overexpressed in BHT 14 and 21 days ($P<0.05$). These findings suggest a progressive remodeling of distal lung parenchyma, an experimental model closer to human pulmonary fibrosis.

BHT regulates remodeling genes/protein overexpression, fibroblasts activation and collagen synthesis

To better understand the mechanisms involved in AECs injury, inflammation, and fibrosis during the time course of BHT- induced lung injury, and to identify candidate genes that might be involved in lung fibrosis, we performed RT-PCR array on whole lung mRNA from control and BHT-treated mice euthanized at 14 and 21 days post-instillation. Consistent with the quantification of fibrosis, total lung collagen content, Col I, Col III and Col V several genes that encode proteins that constitute ECM, such as fibrillary collagens (*COL1A2* and *COL3A1*), and genes that play a role in ECM remodeling, such as matrix metalloproteinases (*MMP3, MMP8, MMP9, MMP14* and *MMP1A*) and specific inhibitors, such as *TIMP4* and *TIMP3* were significantly increased during the fibrotic response and decreased during inflammation (Fig. 3).

Hierarchical clustering of these genes revealed four clusters with distinct gene expression patterns (Fig. 3). *Cluster 1* contained 6 genes grouped in 3 functional categories; among them the most highly represented categories were *CCR2* and *ACTA2*. These genes are involved in the development and progression of lung fibrosis and were downregulated in BHT at day 14, suggesting an expression transition between the pathophysiologic processes of inflammation and remodeling. *Cluster 2* contained 21 genes grouped in 5 functional categories, such as signal transduction that influence inflammation and fibrosis. Among them the most highly represented categories were cytokines (*IL10*), proliferation (*TIMP4, MMP9, SMAD7, EGF)*, apoptosis (*BCL2*) and angiogenesis (*Endothelin*). These genes were downregulated during inflammation and upregulated during fibrosis. *Cluster 3* contained 14 genes grouped in ECM synthesis represented by *LOX, PDGFa, SMAD3* and *TGFB1*. These genes were upregulated during at 21 days fibrotic phase. Cluster 4 contained 7 genes grouped in ECM synthesis and remodeling such as *COL1A2, COL3A1, SMAD4, VEGFA2, MMP1A* and *TIMP2*. These genes were downregulated during 14th day inflammatory phase (Fig. 3).

The most highly represented differences in gene expression between controls and BHT lungs are shown in Fig. 4.

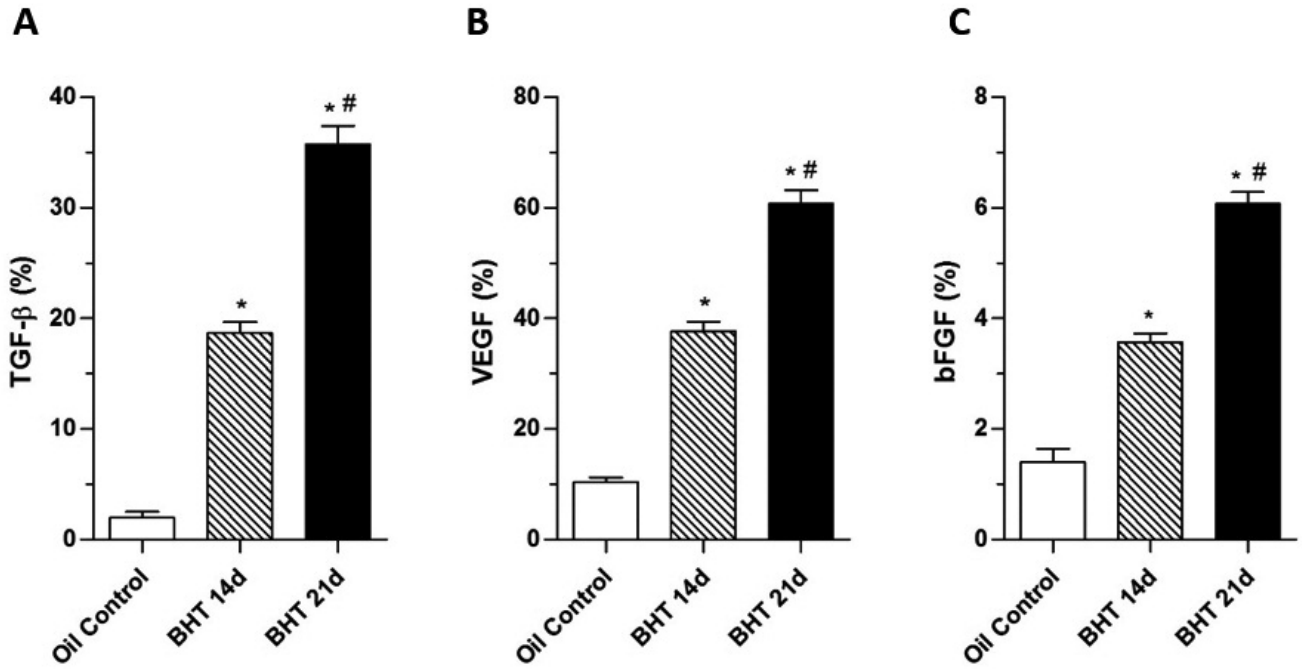

Fig. 2. Immunohistochemistry assessment in lung tissue during the time course of BHT-induced lung fibrosis. **A-C.** Representative box plots of lung tissue sections of saline- and BHT-instilled mice immunostained and quantified by morphometry. **A.** TGF-β expression. **B.** VEGF expression. **C.** bFGF expression. Compared to control critical fibrogenesis-promoting growth factors such as TGF-β, bFGF and VEGF have also significantly overexpressed *in situ* at 14 and 21 days. These findings suggest a progressive remodeling of distal lung parenchyma, an experimental model closer to human pulmonary fibrosis. *Compared to oil control, #compared to BHT14d; $P<0.05$.

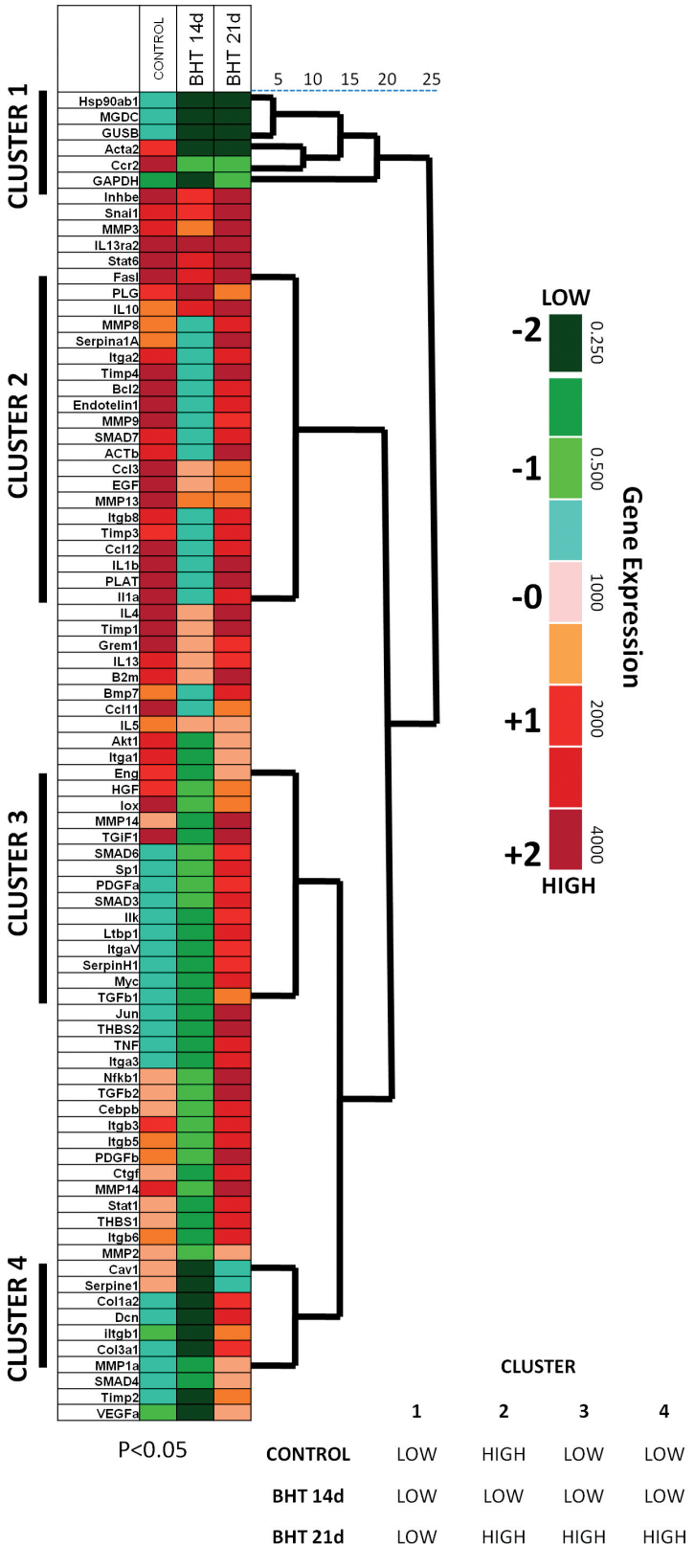

Fig. 3. Gene expression infogram-clustering for time course of BHT-induced lung fibrosis. The gene expression infogram represents most 84 genes that code for inflammation, extracellular matrix components or play a significant role in ECM remodeling. Every row represents a gene and every column a control, 14 and 21 days mouse lung sample. Increased genes are shown in progressively brighter shades of red, and decreased genes are shown in progressively darker shades of green. The baseline per gene was defined as the geometric mean of the expression of the gene in the saline control mice at the initial time point. Consensus tree of unsupervised hierarchical clustering of lung specimens using all probe sets shows horizontal distance representing the correlation of lung samples to one another. Hierarchical clustering of differentially expressed genes revealed four clusters with distinct gene expression patterns. Time-course profiles of cluster 1 shows decreased gene expression in control, BHT 14 day and BHT 21 day groups; cluster 2 shows slight decrease of genes at BHT 14 day coincided with the inflammatory phase; cluster 3 shows progressive increased gene expression at BHT 21 day coincided with the fibrotic phase; and cluster 4 deep decreased gene expression at 14th day inflammatory phase. Genes shown outside of clusters are not different between the groups.

Increased expression and abnormal deposition of Col V is highlighted in final phase of distal pulmonary remodeling

In Figure 5 immunofluorescence for Col I, Col III and Col V on the 14th and 21st day after BHT and control mice is shown. In control and 14 day BHT lungs, Col I fibers are loosely arranged along the basement membrane (BM), assuming a uniform distribution, enhancing alveolar architecture (Fig. 5A-B). In contrast, on day 21 after BHT instillation, significantly thicker Col I fibers are tightly packed along of the BM, modifying the usual histoarchitecture of alveoli when compared to control (Fig. 5C-D; P<0.05). The alveolar septa from 14 and 21 BHT lung exhibits a significant increase of thin Col III fibers irregularly distributed along the BM and involving small vessels when compared to control (Fig. 5F-H; P<0.05). Col V analysis in control shows loose fibers in a homogeneous, linear distribution along the BM and around the vessels (Fig. 5I), consistent with normal lung architecture. In contrast, after 14 and 21 days, BHT exhibits a significant increase of thick Col V fibers assuming an irregular and micronodular distribution involving the BM and small vessels in BHT groups when compared to control (Fig. 5J-L; P<0.05).

Figure 6 (A-I) shows the ultrasctructural characteristics of the alveolar septa from control and BHT animals. Control lungs exhibit alveolar epithelial and endothelial cells with preserved mitochondria, lamellar bodies, endoplasmic reticulum and fibroblast immersed on a thin ECM with homogeneous distribution of the collagen fibers along the alveolar septa (A-C). In contrast, on 14th day BHT lung exhibits a decreased number of lamellar bodies in AECs, distorted mitochondria and endoplasmic reticulum with an increased number of fibroblasts, disarray and prominence of fine and thick collagen fibers, causing a significant thickening of the alveolar septa ECM (D-F). On 21st day, the distribution of immunoreactivity for Col V fibers in alveolar septa is highlighted in fibronexus between the fibroblasts (G-I).

Together, our findings suggest that the alveolar damage by BHT produces a particular inflammatory process to modulate the remodeling phase until it a possible positive feedback can develop between Col V

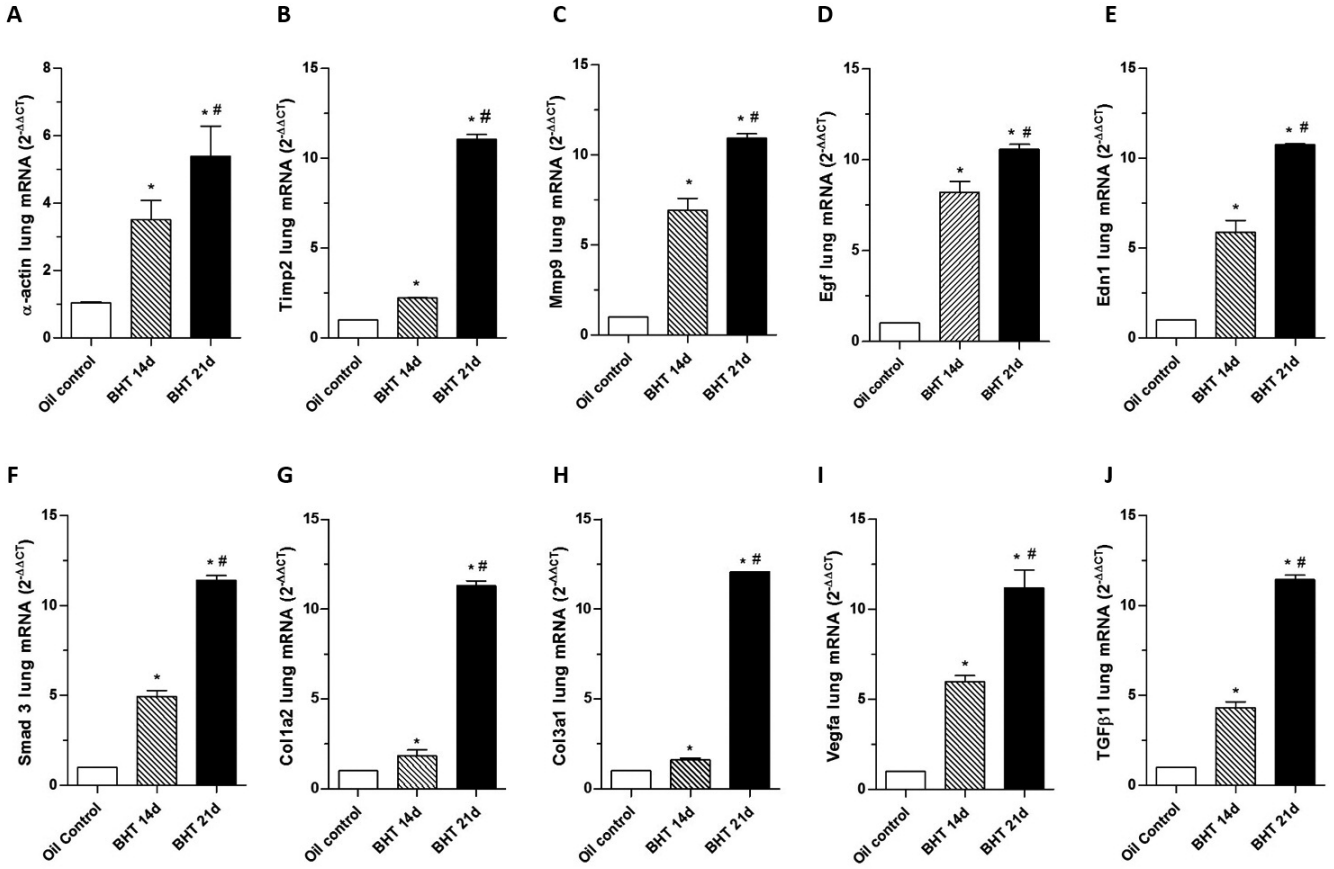

Fig. 4. Gene expression differences between controls and BHT lungs. **A-J.** Expression levels of highly differences in gene expression between controls and BHT lungs are shown in the different boxplots. *Compared to oil control, #compared to BHT14d; P<0.05.

epitope exposing and immune response to favor a progressive lung remodeling and poor outcome (Fig. 7).

Discussion

Investigators have tried improving the experimental fibrosis model to better replicate the histology associated with human idiopathic pulmonary fibrosis (IPF). Bleomycin (BLM), a chemotherapeutic agent, has been the most commonly used agent to induce pulmonary fibrosis in animal models. It induces DNA strand breaks (Sausville et al., 1976; Lown and Sim, 1977), thus leading to epithelial injury, inflammation and ultimately fibrosis. However, the histology from this injury model revealed a proximal airway-centered pattern similar to human airways centered interstitial pneumonia (Churg et al., 2004), different from the distal parenchyma compromised in human IPF. Butylated hydroxytoluene (BHT) is a quinone that cleaves DNA strands through oxygen radicals and accumulates predominantly in the lung inducing epithelial and endothelial cell damage (Haschek et al., 1983; Parra et al., 2008), which is followed by inflammation and proliferation of pulmonary parenchymal cells. In the present study, we found that BHT alters distal airway/alveolar epithelial cells and extracellular matrix signaling involved in the activation and perpetuation of fibrosis in a different pathway from airway-centered BLM lung fibrosis (Cabrera et al., 2013).

In the current study, BHT induced alveolar collapse, honeycombs, hyperplastic AEC2, and progressive increase of the profibrotic factor and genes with evident distal response in a similar pattern of human IPF (Katzenstein et al., 2008). Specifically, we found that BHT injury increased fibrotic-related gene overexpression such as *PDGFα* and *SMAD3-SMAD6*, leading to myofibroblastic activation. Consequently, the increased peripheral production of ECM triggers a highlighted lung remodeling in the distal microenvironment. In addition, Col V, unique immunogenic fibrillar collagen (Parra et al., 2006; Ogido et al., 2008), is overexpressed in an abnormal bundle

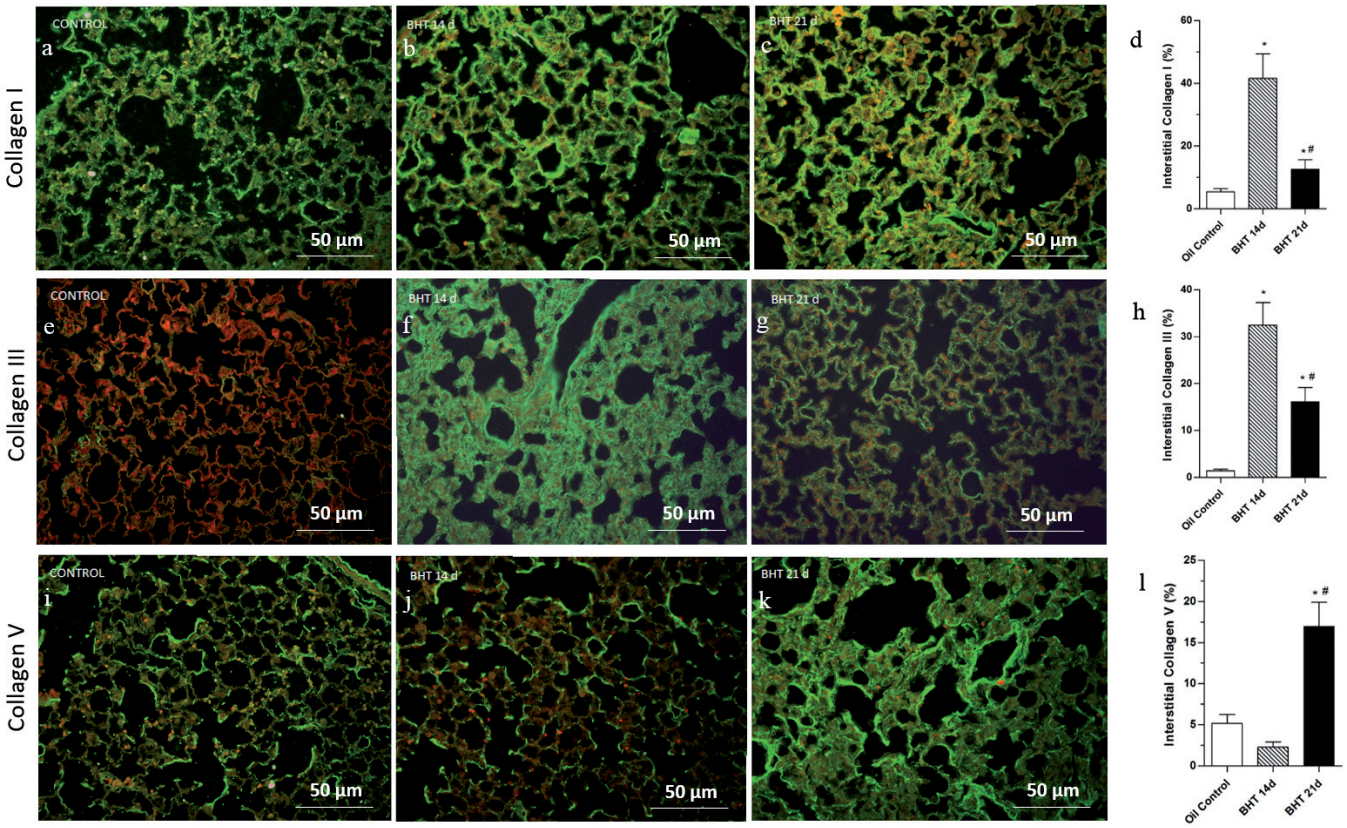

Fig. 5. Immunofluorescence assessment of collagen I, III and V in lung tissue during the time course of BHT-induced lung fibrosis. Representative micrographs in lung tissue sections of saline- and BHT-instilled mice stained with immunofluorescence, counterstained with Blue Evans in red. **A, E, I.** Saline-instilled mouse. **B, F, J, C, G, K.** BHT-instilled mice at 14 and 21 days, respectively. **A, E, I.** Immunofluorescence shows weak green birefringence of Col I, Col III and Col V in alveolar walls from the control groups. **B, F, J, C, G, K.** Pulmonary specimens of BHT 14 and BHT 21 show diffuse increase of Col I, Col III and Col V green birefringence in alveolar walls. **D, H, L.** Col I, Col III and Col V quantitation. *Compared to oil control, #compared to BHT14d; P<0.05. Scale bars: 50 *µ*m.

manner in the late stage (21d). This may explain the increase of the IL-17 cytokine which promotes a Th17-response against Col V and reported in similar works done by Braun (2009) and Fabro (2015) (Braun et al., 2009; Fabro et al., 2015). Fabro and colleagues (Fabro et al., 2015) also suggested that, after 21 days of initial and unique epithelial/endothelial lung injury, distal myofibroblastic activation lead to production of ECM,

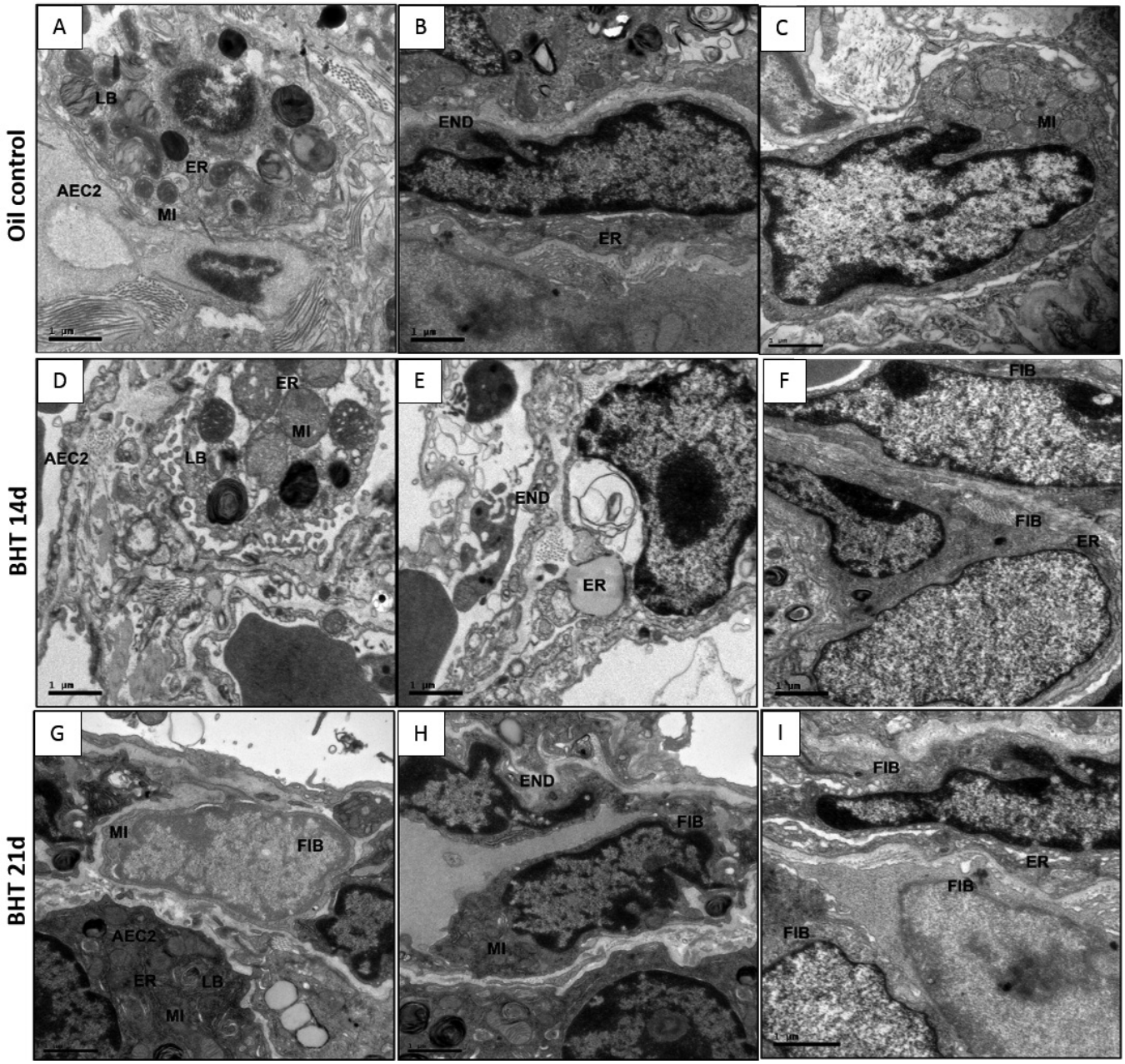

Fig. 6. Electron microscopy assessment in lung tissue during the time course of BHT-induced lung fibrosis. **A-I.** Representative electron micrographs in lung tissue sections of saline- and BHT-instilled mice stained with uranyl acetate and lead citrate. **A-C.** Saline-instilled mouse. **D-I.** BHT-instilled mice at 14 and 21 days, respectively. **A-I.** Transmission electron microscopy shows the submicroscopic structure of the alveolar septa from control and BHT animals. **A-C.** Control lung exhibit type 2 alveolar epithelial (AECs) and endothelial cells (ECs) with preserved mitochondria (MI), endoplasmic reticulum (ER), lamellar bodies (LB) and fibroblast (FIB) immersed on a thin ECM with homogeneous distribution of the collagen fibers along the alveolar septa. **D-F.** On 14th day BHT lung exhibits distorted mitochondria (MI) and endoplasmic reticulum (ER) of epithelial (AECs) and endothelial cells (ECs) with decreased number of lamellar bodies (LB) and increased number of fibroblasts (FIB) with disarray and prominence of fine and thick collagen fibers, causing a significant thickening of the ECM. **G-I.** On 21st day, the distribution of immunoreactivity for Col V fibers in alveolar septa is highlighted in fibroblasts (FIB). Scale bars: 1 μm.

which in the late stage is related Th-17 autoimmunity to Col V.

In the present study, determination of remodeling regulated genes expression patterns associated with the progression of the fibrotic response highlighted the above results. A number of genes implicated in the ECM remodeling were upregulated during the development of BHT induced fibrosis. These including genes are involved in the development and progression of lung fibrosis (*LOX, MMP-2, MMP-9 and TIMP1, TGF-β1, SMAD2* and *SMAD3*), transcription activator activity, intracellular signaling cascade, phosphoprotein, acetylation, and cytoskeleton (*CBPP, STAT-11, STAT-6* and *NFKb1*), ECM synthesis, chemotaxis, angiogenesis, proliferation and apoptosis (*TNF, IL-1b* and *IL-3, CTGF, EGF* and *VEFGA*) and profibrotic (*ACTA2, SNAIL1* and *GREM1*). As expected, this expression profile contrasts to that found in BLM lung fibrosis where the most enriched pathways included genes involved in cell cycle and in regulation of transcription, including *fibromodulin,* and *tenascin-C, MMP-8, Ccr1* and *Cxcr7, Adducin 1, actin-bundling protein 1,* and *Caldesmon 1, interferon (alpha and beta) receptor 2 (Ifnar2)* and *the chemokine Cxcl417*.

Several studies have demonstrated that increased expression of FGF and VEGF proteins plays a critical role in the development of experimental lung fibrosis (Kim et al., 2016; Venkatadri et al., 2017). Moreover, TGF-β1 protein induces a strong inhibition of FGF-1 in myofibroblasts in contrast to strong expression of both, suggesting that differences in the fibrotic response might be in part due to the other mechanisms as a Th17 response (Peng et al., 2014). On the other hand, FGF may promote survival and migration of fibroblast (Joannes et al., 2016) and VEGF have been recently implicated disease progression and mortality in idiopathic pulmonary fibrosis (Venkatadri et al., 2017).

Increased TGF- β1 gene expression has been widely implicated in the development and progression of pulmonary fibrosis and, through an intricate signaling cascade, promotes the transcription of Col I and fibronectin in fibroblasts. A family of transcription factors, the so called Smad proteins (Heldin et al., 1997), mediates the intracellular signaling pathway downstream to the TGF- β1 receptors. The signaling process begins when a TGF-β protein attaches to a receptor on the cell

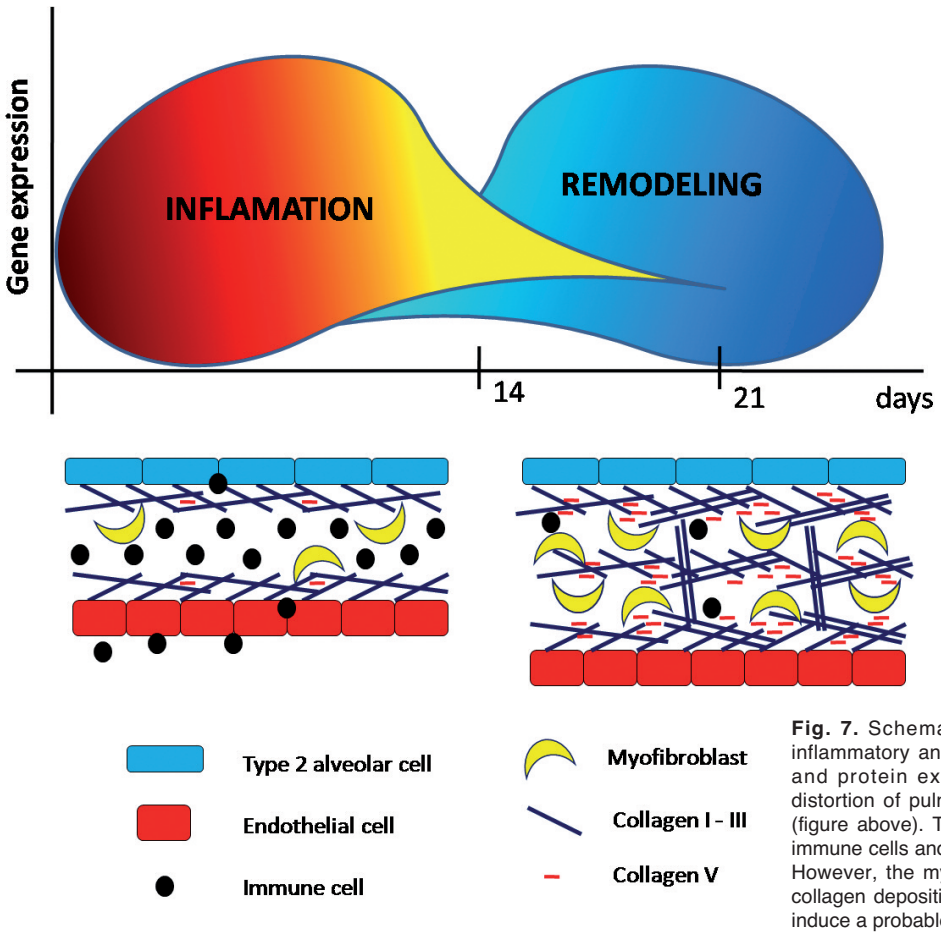

Fig. 7. Schematic pathophysiologic balance between inflammatory and remodeling phases. Note that the gene and protein expression profile favor an architectural distortion of pulmonary microenvironment after lung injury (figure above). The inflammatory phase shows an influx of immune cells and intact connective framework (left schema). However, the myofibroblasts and abnormal and increased collagen deposition favor exposing of collagen V epitope to induce a probable immune response (right schema).

surface, which activates Smad 3 protein. In the nucleus, the Smad protein complex binds to specific areas of DNA to control the activity of particular genes and regulate cell proliferation (Heldin et al., 1997).

Another upregulated transcript gene we found was *NFκB2*, a member of the *NFκB* family of transcription factors. *NFκB2* present an important role in inflammation and, current genetic confirmation indicates that negative feedback control mechanisms are necessary to limit the inflammatory effect of sustained activation of *NFκB2* signaling (Yang et al., 2010). Remarkably, although NFkB2 is central in inflammation, we found (realtime-PCR) that it was highly increased during the fibrotic response.

In the current study, we found that up-regulation of cytokines and growth factor proteins and genes induced by BHT resulted in an increase in total and specific types of lung collagen accumulation in lungs. It is interesting to observe the progressive increase of total collagen from day 14 to day 21 stage of fibrotic response. Increases of the same magnitude in collagen content were previously reported in experimental BLM-induced pulmonary fibrosis (Starcher et al., 1978) and paraquat poisoning (Wilson and Wynn, 2009). As expected, Col I and Col III increased on day 14 and 21 after BHT treatment, coincident with elastic fibers decrease.

Interestingly, we demonstrated that Col V was distorted and over deposited mainly on day 21 in BHT lungs. The epithelial and endothelial cell abnormalities caused by BHT injury suggest that the denuded BM exposure Col V epitopes increasing the synthesis of these cells, along with fibroblasts and myofibroblasts, which in turn is associated with the development of anti-Col V immunity (Vittal et al., 2013). Col V induced tolerance suppresses collagen deposition, TGF-β and associated transcripts in pulmonary fibrosis (Vittal et al., 2013). The immune response results in deregulated tissue healing, accelerating fibrosis and accumulation of ECM components (Wilson and Wynn, 2009), with myofibroblast differentiation and increase of cytokines, such as TGF- β production (Sime et al., 1997; Sueblinvong et al., 2012). Our group previously observed an increased Col V accumulation in lungs of systemic sclerosis patients and rabbit model (Teodoro et al., 2004; Parra et al., 2009, 2010). Wilkes group (Vittal et al., 2013) recently demonstrated that nebulized Col V prevented BLM-induced fibrosis, collagen deposition, and myofibroblast differentiation. In a clinically relevant established model, nebulized Col V decreased collagen deposition and mRNA array revealed down-regulation of genes specific to fibrosis such as TGF- β.

We suggest that BHT alters gene expression profile promoting distal lung remodeling by Col V eventually driving an IL-17 response. This mechanism involves molecular signaling of the initiation and progression of pulmonary fibrosis highlighted similarities to human IPF in a pathway related to overexpression of Col V and remodeling regulated genes/proteins, thus arising as a promissory model to identify effective therapeutic targets.

Acknowledgements. The authors gratefully acknowledge support from The National Council for Scientific and Technological Development [CNPq-471939/2010-2 and 483005/2012-6]; Foundation for the Support of Research of the State of São Paulo [FAPESP 12/03543-2, FAPESP 11/09181-2, FAPESP 2012/07040-5, FAPESP 2013/05886-7], Laboratories for Medical Research [LIMs], Hospital das Clinicas, University of São Paulo Medical School and Coordination for the Improvement of Higher Level Personnel (CAPES).
Disclosure statement. No competing financial interests exist.

References

Birk D.E., Fitch J.M., Babiarz J.P., Doane K.J. and Linsenmayer T.F. (1990). Collagen fibrillogenesis in vitro: interaction of types I and V collagen regulates fibril diameter. J. Cell Sci. 95, 649-657.

Braun R.K., Molitor-Dart M., Wigfield C., Xiang Z., Fain S.B., Jankowska-Gan E., Seroogy C.M., Burlingham W.J., Wilkes D.S., Brand D.D., Torrealba J. and Love R.B. (2009). Transfer of tolerance to collagen type V suppresses T-helper-cell-17 lymphocyte-mediated acute lung transplant rejection. Transplantation 88, 1341-1348.

Cabrera S., Selman M., Lonzano-Bolaños A., Konishi K., Richards T.J., Kaminski N. and Pardo A., (2013). Gene expression profiles reveal molecular mechanisms involved in the progression and resolution of bleomycin-induced lung fibrosis. Amer. J. Physiol. Lung Cell. Mol. Physiol. 304, L593-601.

Churg A., Myers J., Suarez T., Gaxiola M., Estrada A., Mejia M. and Selman M, (2004). Airway-centered interstitial fibrosis: a distinct form of aggressive diffuse lung disease. Am. J. Surg. Pathol. 28, 62-68.

Fabro A.T., da Silva P.H., Zocolaro W.S., de Almeida M.S., Rangel M.P., de Oliveira C.C., Minatel I.O., Prando E.D., Rainho C.A., Teodoro W.R., Velosa A.P., Saber A.M., Parra-Cuentas E.R., Popper H.H. and Capelozzi V.L. (2015). The Th17 pathway in the peripheral lung microenvironment interacts with expression of collagen V in the late state of experimental pulmonary fibrosis. Immunobiol. 220, 124-135.

Gelse K., Poschl E. and Aigner T. (2003). Collagens: structure, function and byosynthesis. Adv. Drug Deliv. Rev. 55, 1531-1546.

Gundersen H.G., Bendtsen T.F., Korbo L., Marcussen N., Moller A., Nielsen K., Nyengaard J.R., Pakkenberg B., Sorensen F.B., Vesterby A. and West M.J. (1988). Some new, simple and efficient stereological methods and their use in pathological research and diagnosis. APMIS 96, 379-394.

Haschek W.M., Reiser K.M., Klein-Szanto A.J., Keher J.P., Smith L.H., Last J.A. and Witschi H.P. (1983). Potentiation of butylated hydroxytoluene-induced acute lung damage by oxygen. Cell kinetics and collagen metabolism. Am. Rev. Respir. Dis. 127, 28-34.

Heldin C.H., Miyazono K. and Dijke P. (1997). TGF-beta signalling from cell membrane to nucleus through SMAD proteins. Nature 390, 465-471.

Joannes A., Brayer S., Besnard V., Marchal-Sommé J., Jaillet M., Mordant P., Mal H., Borie R., Crestani B. and Mailleux A.A. (2016). FGF9 and FGF18 in idiopathic pulmonary fibrosis promote survival and migration and inhibit myofibroblast differentiation of human lung fibroblasts in vitro. Am. J. Physiol Lung Cell. Mol. Physiol. 310, L615-629.

Katzenstein A.L., Mukhopadhyay S. and Myers J.L. (2008). Diagnosis of usual interstitial pneumonia and distinction from other fibrosing interstitial lung diseases. Hum. Pathol. 39, 1275-1294.

Kim K.K., Sisson T.H. and Horowitz J.C. (2017). Fibroblast Growth Factors and Pulmonary Fibrosis: It's more complex than it sounds. J. Pathol. 241, 6-9.

Konomi H., Hayashi T., Nakayasu K. and Arima M. (1984). Localization of type V collagen and type IV collagen in human cornea, lung, and skin. Immunohistochemical evidence by anti-collagen antibodies characterized by immunoelectroblotting. Am. J. Pathol. 4, 116, 417-426.

Lown J.W. and Sim S.K. (1977). The mechanism of the bleomycin-induced cleavage of DNA. Biochem. Biophys. Res. Commun. 77, 1150-1157.

Ogido L.T., Teodoro W.R., Velosa A.P., de Oliveira C.C., Parra E.R., Capelozzi V.L. and Yoshinari N.H. (2008). Abnormal collagen deposition in synovia after collagen type V immunization in rabbits. Histol. Histopathol. 23, 263-269.

Pardo A. and Selman M. (2002). Molecular mechanisms of pulmonary fibrosis. Front. Biosci. 7, d1743-d1761.

Parra E.R., Teodoro W.R., Velosa A.P., de Oliveira C.C., Yoshinari N.H. and Capelozzi V.L. (2006). Interstitial and vascular type V collagen morphologic disorganization in usual interstitial pneumonia. J. Histochem. Cytochem. 54, 1315-1325.

Parra E.R., Boufelli G., Bertanha F., Samorano L de P., Aguiar A.C. Jr, Costa F.M., Capelozzi V.L. and Barbas-Filho J.V. (2008). Temporal evolution of epithelial, vascular and interstitial lung injury in an experimental model of idiopathic pulmonary fibrosis induced by butyl-hydroxytoluene. Int. J. Exp. Pathol. 89, 350-357.

Parra E.R., Aguiar Jr. A.C., Teodoro W.R., de Souza R., Yoshinari N.H. and Capelozzi V.L. (2009). Collagen V and vascular injury promote lung architectural changes in systemic sclerosis. Clin. Respir. J. 3, 135-142.

Parra E.R., Teodoro W.R., de Morais J., Katayama M.L., de Souza R., Yoshinari N.H. and Capelozzi V.L. (2010). Increased mRNA expression of collagen V gene in pulmonary fibrosis of systemic sclerosis. Eur. J. Clin. Invest. 40,110-120.

Peng X., Moore M.W., Peng H., Sun H., Gan Y., Homer R.J. and Herzog E.L. (2014). CD4+CD25+FoxP3+ Regulatory Tregs inhibit fibrocyte recruitment and fibrosis via suppression of FGF-9 production in the TGF-beta1 exposed murine lung. Front. Pharmacol. 5, 80.

Roulet M., Ruggiero F., Karsenty G. and LeGuellec D. (2007). A comprehensive study of the spatial and temporal expression of the col5a1 gene in mouse embryos: a clue for understanding collagen V function in developing connective tissues. Cell Tissue Res. 327, 323-332.

Sausville E.A., Peisach J. and Horwitz S.B., (1976). A role for ferrous ion and oxygen in the degradation of DNA by bleomycin. Biochem. Biophys. Res. Commun. 73, 814-822.

Sime P.J., Xing Z., Graham F.L., Csaky K.G. and Gauldie J. (1997). Adenovector-mediated gene transfer of active transforming growth factor-beta1 induces prolonged severe fibrosis in rat lung. J. Clin. Invest. 100, 768-767.

Song K.H., Kim M.Y., Jang S.J., Colby T.V. and Kim D.S. (2009). Pathologic and radiologic differences between idiopathic and collagen vascular disease-related usual interstitial pneumonia. Chest 136, 23-30.

Starcher B.C., Kuhn C. and Overton J.E. (1978). Increased elastin and collagen content in the lungs of hamsters receiving an intratracheal injection of bleomycin. Am. Rev. Respir. Dis. 117, 299-305.

Sueblinvong V., Neujahr D.C., Mills S.T., Roser-Page S., Ritzenthaler J.D., Guidot D., Rojas M. and Roman J. (2012). Predisposition for disrepair in the aged lung. Amer. J. Med. Sci. 344, 41-51.

Teodoro W.R., Velosa A.P., Witzel S.S., Garippo A.L., Farhat C., Parra E.R., Sonohara S., Capelozzi V.L. and Yoshinari N.H. (2004). Architectural remodelling in lungs of rabbits induced by type V collagen immunization: a preliminary morphologic model to study diffuse connective tissue diseases. Pathol. Res. Pract. 200, 681-691.

Venkatadri R., Iyer A.K., Ramesh V., Wrigth C., Castro C.A., Yakisich J.S. Azad N. (2017). MnTBAP inhibits bleomycin-induced pulmonary fibrosis by regulating VEGF and Wnt signaling. J. Cell. Physiol. 232, 506-516.

Vittal R., Mickler E.A., Fisher A.J., Zhang C., Rothhaar K., Gu H., Brown K.M., Emtiazdjoo A., Lott J.M., Frye S.B., Smith G.N., Sandusky G.E., Cummings O.W. and Wilkes D.S. (2013). Type V collagen induced tolerance suppresses collagen deposition, TGF-beta and associated transcripts in pulmonary fibrosis. PloS one 8, e76451.

Yang L., Cui H., Wang Z., Zhang B., Ding J., Liu L. and Ding H.F. (2010). Loss of negative feedback control of nuclear factor-kappaB2 activity in lymphocytes leads to fatal lung inflammation. Am. J. Pathol. 176, 2646-2657.

Weibel E.R. (2017). Lung morphometry: the link between structure and function. Cell Tissue Res. 367, 413-426.

Wilson M.S. and Wynn T.A. (2009). Pulmonary fibrosis: pathogenesis, etiology and regulation. Muc. Immunol. 2, 103-121.

Accepted June 5, 2018